



**HAL**  
open science

## Molecular strategies for adapting *Bacillus subtilis* 168 biosurfactant production to biofilm cultivation mode

Hannah Luise Bruck, Frank Delvigne, Pascal Dhulster, Philippe Jacques, François Coutte

### ► To cite this version:

Hannah Luise Bruck, Frank Delvigne, Pascal Dhulster, Philippe Jacques, François Coutte. Molecular strategies for adapting *Bacillus subtilis* 168 biosurfactant production to biofilm cultivation mode. *Bioresource Technology*, 2019, 293, 10.1016/j.biortech.2019.122090 . hal-02623519

**HAL Id: hal-02623519**

**<https://hal.inrae.fr/hal-02623519>**

Submitted on 20 Jul 2022

**HAL** is a multi-disciplinary open access archive for the deposit and dissemination of scientific research documents, whether they are published or not. The documents may come from teaching and research institutions in France or abroad, or from public or private research centers.

L'archive ouverte pluridisciplinaire **HAL**, est destinée au dépôt et à la diffusion de documents scientifiques de niveau recherche, publiés ou non, émanant des établissements d'enseignement et de recherche français ou étrangers, des laboratoires publics ou privés.



Distributed under a Creative Commons Attribution - NonCommercial 4.0 International License

Original research paper

**Molecular strategies for adapting *Bacillus subtilis* 168 biosurfactant production to biofilm cultivation mode**

Hannah Luise Brück<sup>1,2</sup>, Frank Delvigne<sup>1</sup>, Pascal Dhulster<sup>2</sup>, Philippe Jacques<sup>1</sup>, François Coutte<sup>2\*</sup>

<sup>1</sup>MiPI, TERRA Teaching and Research Centre, Gembloux Agro-Bio Tech, University of Liège, Avenue de la Faculté, 2B, B-5030, Gembloux, Belgium

<sup>2</sup>Univ. Lille, INRA, ISA, Univ. Artois, Univ. Littoral Côte d'Opale, EA 7394 - ICV - Institut Charles Viollette, F-59000 Lille, France

\*Corresponding author: Dr. François Coutte

E-mail: francois.coutte@univ-lille.fr

## **Abstract**

Biofilm bioreactors have already been proven to be efficient systems for microbial lipopeptide production since they avoid foam formation. However, the cell adhesion capacities of the laboratory strain *B. subtilis* 168 to the biofilm bioreactor support are limited. In this work, we present a novel approach for increasing cell adhesion through the generation of filamentous and/or exopolysaccharide producing *B. subtilis* 168 mutants by genetic engineering. The single cell growth behavior was analyzed using time-lapse microscopy and the colonization capacities were investigated under continuous flow conditions in a drip-flow reactor. Cell adhesion could be increased three times through filamentous growth in lipopeptide producing *B. subtilis* 168 derivatives strains. Further restored exopolysaccharide production increased up to 50 times the cell adhesion capacities. Enhanced cell immobilization resulted in 10 times increased surfactin production. These findings will be of particular interest regarding the design of more efficient microbial cell factories for biofilm cultivation.

**Keywords:** *Bacillus subtilis*, biofilm bioreactor, filamentation, cell adhesion, surfactin

## 1   **1   Introduction**

2   The gram-positive soil bacterium *Bacillus subtilis* produces naturally different classes of  
3   lipopeptides as secondary metabolites (Jacques, 2011). These lipopeptides combine remarkable  
4   physicochemical properties and biological activities and thus have a wide range of applications  
5   in various fields (Jacques, 2011). **Since** lipopeptides are very powerful **biosurfactants**, the  
6   bioreactor design and operating conditions have to be chosen properly in order to control or to  
7   avoid foam formation (Coutte et al., 2017).

8   Innovative lipopeptide production processes avoiding foam formation based on an air/liquid  
9   membrane contactor (Coutte et al., 2013, 2010b) and on a trickle-bed biofilm reactor (Zune et  
10  al., 2017, 2013) have been developed in previous works. Both systems have shown to promote  
11  biofilm formation. In the first system, a **thin surfactin producing biofilm** has been developed by  
12  *B. subtilis* **168** derivative strains on the **air/liquid membrane contactor** (Coutte et al., 2013). In  
13  the second system, the reactor contains a metal structured packing that provides a high specific  
14  surface area for the cell adhesion and biofilm development (Zune et al., 2013). In **this trickle-**  
15  **bed biofilm reactor**, natural filamentous microorganism such as the fungi *Aspergillus oryzae*  
16  and *Trichoderma reesei* have shown to have much better cell adhesion capacities than the natural  
17  non-filamentous and lipopeptide producing bacterial strain *Bacillus amyloliquefaciens* (Khalesi  
18  et al., 2014; Zune et al., 2015, 2013). Other interesting biofilm-based processes consisting of a  
19  rotating disc reactor (Chtioui et al., 2012) or an inverse fluidized bed bioreactor (Fahim et al.,  
20  2013) have shown that the lipopeptide productivity could be increased through cell  
21  immobilization.

22  Biofilm bioreactors provide increased productivity and process stability through the generation  
23  of a highly active attached biomass with a high resistance to external influences and toxic  
24  compounds (Ercan and Demirci, 2015). Especially for surfactin production, biofilm bioreactors  
25  **can be** conducive, since surfactin is linked to the biofilm regulation mechanism as a trigger  
26  molecule for the expression of matrix genes (Mielich-Süss and Lopez, 2015).

27 The *B. subtilis* wild-type strain NCIB3610 forms robust and highly structured biofilms on solid  
28 surfaces and air/liquid interfaces (Kearns et al., 2005), whereas the widely used laboratory strain  
29 *B. subtilis* 168 forms only thin and relatively undifferentiated biofilms (Branda et al., 2004).  
30 McLoon et al. (2011) have shown that several genetic mutations in *B. subtilis* 168, which have  
31 accumulated during the domestication process, contribute to impaired biofilm formation.  
32 Especially, a deficiency in exopolysaccharide (EPS) production, due to a point mutation in the  
33 *epsC* gene, is responsible for a strongly reduced matrix production (McLoon et al., 2011).  
34 Another known alteration is the defective *sfp* gene (McLoon et al., 2011). The gene *sfp* codes  
35 for a phosphopantetheine-transferase, which is essential for the non-ribosomal peptide synthesis  
36 of lipopeptides such as surfactin (Coutte et al., 2010a; McLoon et al., 2011). The defective  
37 biofilm formation is a limiting factor for a robust colonization of the biofilm bioreactor support  
38 by *B. subtilis* 168 derivatives strains. For a good bioreactor performance, enhanced support  
39 colonization capacities are necessary. In wild-type strains of *B. subtilis*, architecturally complex  
40 biofilm structures are associated with the growth in chains of cells that are bound together in  
41 bundles via exopolysaccharides (Kearns et al., 2005). Focusing on the spatial organization of  
42 the cells in the biofilm, it might be possible to improve the support colonization through the  
43 engineering of cell shapes.

44 Numerous metabolic engineering strategies have been already developed to design more  
45 efficient cell factories (Volke and Nikel, 2018). The manipulation of cell shapes has been rarely  
46 exploited to optimize bioprocesses (Volke and Nikel, 2018). Gene deletions affecting the cell  
47 division induce morphological changes in cells. In *B. subtilis*, the cell septation protein SepF  
48 has shown to be involved in the septum formation and is required for a later step in cell division  
49 but does not represent an essential gene (Hamoen et al., 2006). The deletion of SepF perturbs  
50 the division septum assembly in the cells and thus provokes filamentous growth due to a  
51 deficiency in cell division (Hamoen et al., 2006). Recently, Zhao et al. (2018) have deleted  
52 several genes related to peptidoglycan hydrolases in a *B. subtilis* strain leading to elongated  
53 bacterial cells with increased specific growth rates and improved enzyme production capacities.

54 In this work, we investigate different possibilities of engineering *B. subtilis* 168 strains to  
55 improve the cell adhesion capacities **through the change of cell shape and enhanced biofilm**  
56 **matrix production**. The goal is to be able to produce surfactin in a continuous bioprocess with  
57 **immobilized** cells on a reactor support through the formation of a structural organized biofilm.  
58 In the first step, the engineered strains are characterized at single cell level with a time lapse  
59 microscope to evaluate their growth dynamic. Then, the colonization and adhesion capacities of  
60 the engineered strains are tested under more real conditions in a drip-flow reactor (DFR) with  
61 continuous flow. Images with a live camera are taken to establish a cell colonization and  
62 biofilm formation model. Moreover, the surfactin production capacity of the adhered cells is  
63 analyzed. Based on the results, we discuss the impact of filamentous growth, surfactin  
64 production and biofilm formation on the performance of biofilm-based bioprocesses.

## 65 **2 Materials and methods**

### 66 **2.1 Strains and strain construction**

67 All genetically engineered strains that were used in this study are derived from the laboratory  
68 strain *B. subtilis* 168 (*trpC2*). The strains have been selected and/or modified focusing on three  
69 genetic modifications: the introduction or respectively the restoration of the genes *sfp* and *epsC*  
70 as well as the deletion of *sepF*. For a complete list of the strains and their corresponding  
71 genotype as well as the plasmid used in this work see Table 1.

72 For the transformation, *B. subtilis* strains have been grown in natural competence medium  
73 (14 g/L  $K_2HPO_4 \cdot 3H_2O$ , 5.3 g/L  $KH_2PO_4$ , 20 g/L Glucose, 8.8 g/L Tri-Na Citrate, 0.22 g/L  
74 Ferric- $NH_4$ -citrate, 1g casein hydrolysate, 2 g K glutamate, 1 M  $MgSO_4$ , 1.6 mg/L tryptophan)  
75 at 37°C and 160 rpm to favor the DNA uptake and integration. Selective media were prepared  
76 by adding various antibiotics to lysogeny broth (LB) (10 g/L tryptone, 5g/L yeast extract,  
77 10 g/L NaCl) or LB containing 1.7% agar: chloramphenicol (Cm) 5 µg/mL, neomycin (Neo)  
78 5 µg/mL, erythromycin (Erm) 1 µg/mL, spectinomycin (Spc) 100 µg/mL.

79 In *sfp+* *B. subtilis* 168 mutants, a functional *sfp* gene has been inserted into the *amyE* locus  
80 through homologous recombination of the plasmid pBG129, as previously described (Coutte et  
81 al., 2010a). Positive clones, showing a chloramphenicol-resistance and spectinomycin  
82 sensibility due to a double cross-over homologous recombination of pBG129, were selected. A  
83 correct *sfp* gene transformation was further confirmed by a positive hemolytic test due to the  
84 presence of surfactin and negative amylase activity test as a result of the successful insertion of  
85 *sfp* into the *amyE* locus. Moreover, surfactin production of the *Sfp+* strains was verified in  
86 planktonic cultures using reversed-phase UPLC-MS analysis (see section 2.7).

87 The gene deletion of *sepF* was performed by using the gene deletion strategy “Pop in – pop  
88 out”, previously described by Tanaka et al. (2012). Based on this technique, a master strain was  
89 constructed by replacing the *upp* gene with a neomycin resistance gene under the control of the  
90 Lambda Pr promoter ( $\lambda$ Pr-Neo) through homologous recombination of the plasmid pBG402.  
91 Positive clones with a neomycin-resistance were selected. In the following, the gene deletions  
92 were introduced in the master strain through homologous recombination of the targeted gene  
93 sequence *sepF* with the gene deletion cassette. The gene deletion cassette was synthesized by  
94 polymerase chain reaction (PCR) through the assemblage of different components: the up and  
95 down stream element of the gene to be deleted (*sepF*) and the element containing a phleomycin  
96 resistance gene, the repressor gene of the Lambda promoter *cI* which is necessary for  
97 counterselection. Positive clones, showing a phleomycin resistance and neomycin sensitivity as  
98 a result of the cassette insertion, were selected. All genetic manipulations have been verified by  
99 PCR-based assays and the sequencing of the manipulated gene segment. Figure 1 summarizes  
100 the different genetic modification strategies and their corresponding outcome for adapting  
101 *B. subtilis* 168 surfactin production to biofilm cultivation mode.

## 102 **2.2 Time-lapse microscopy analysis of single *B. subtilis* cells**

103 The cell morphology and growth behavior at single cell level was analyzed using an inverted  
104 phase-contrast time lapse microscope system (Eclipse Ti2, Nikon Instruments Europe BV,

105 Amsterdam, Netherlands). The *B. subtilis* pre-cultures and agar pads were exactly prepared as  
106 described in the article of Jong et al. (2011). The pre-cultures were diluted to an OD<sub>600nm</sub> of 0.03  
107 and the cells of the mutants were deposited on the solid agar surface. The microscope slide with  
108 the agar pad and the loaded cells was incubated at 37°C during 1h prior to the microscope  
109 analysis. The prepared microscope slide was then placed on the pre-heated (37°C) microscope  
110 table and 100x oil immersion objective. The cell development of selected single cells was then  
111 followed in real-time during 8h. Images were taken each 12 minutes.

### 112 **2.3 Drip-flow reactor composition and growth conditions**

113 For the cell adhesion capacity analysis, biofilms were grown on silicone coupons in six parallel  
114 flow chambers per DFR (six-chamber Drip Flow Biofilm Reactor®, Biosurface Technologies  
115 Corporation, Montana, USA). The DFR facilitates the observation of biofilm initiation and  
116 spreading on a solid surface (called coupon) under low shear stress conditions. In our case, we  
117 used silicone coupons with a rough surface to increase the specific surface area that will be  
118 available for the initial cell adhesion and biofilm formation. The surface structure image of the  
119 silicone coupon was recorded with a 3D high resolution digital microscope VHX-6000  
120 (KEYENCE International Belgium NV/SA, Mechelen, Belgium).

121 The strains were cultivated in Landy MOPS medium at pH 7.0 (20 g/L glucose, 5 g/L glutamic  
122 acid, 1 g/L yeast extract, 0.5 g/L MgSO<sub>4</sub>, 1 g/L K<sub>2</sub>HPO<sub>4</sub>, 0.5 g/L KCl, 1.6 mg/L CuSO<sub>4</sub>,  
123 1.2 mg/L MnSO<sub>4</sub>, 0.4 mg/L FeSO<sub>4</sub>, 21 g/L MOPS, 1.6 mg/L tryptophan). The DFR was placed  
124 in a cell culture room kept at 37°C. For the inoculation, overnight cultures of the engineered  
125 strains grown in Landy MOPS medium at 37° and 160 rpm were diluted with Landy MOPS  
126 medium to an OD<sub>600nm</sub> of 1. The reactor was kept horizontally and 20 mL of the diluted culture  
127 was injected per chamber with a syringe. The inoculation has been followed by a 6h batch phase  
128 permitting the cells to settle down and adhere on the support. After the batch phase, the reactor  
129 was inclined and the continuous phase with the delivery of fresh medium was launched with a  
130 flow rate of ~13 mL/h per chamber during 42h, resulting in a total incubation time of 48h. For



131 each mutant the cell adhesion capacity has been analyzed with 1 to 3 technical replicates per  
132 experiment that has been repeated at least 3 times (biological replicates).

#### 133 **2.4 Cell counting after initial adhesion on the drip-flow reactor support**

134 To determine the initial adhesion capacities of the mutants, the strains were cultivated and  
135 inoculated in the DFR as previously described (cf. 2.3). After 6h of batch phase, a continuous  
136 flow (~13 mL/h) was launched during 1h to flush gently non-attached cells from the coupons.  
137 Then, the coupons were taken out of the chambers and put into a 50 mL Falcon tube containing  
138 10 mL of phosphate-buffered saline (PBS). After vigorous vortexing, ten-fold dilution series  
139 from  $10^0$  to  $10^{-6}$  were performed with the cell solutions. From each dilution, 100  $\mu$ L of the cell  
140 solution was dropped and plated on LB agar Petri dishes. The Petri dishes were incubated  
141 overnight at 37°C. The developed colony were counted to estimate the number of viable  
142 adhered cells on the coupon surface. The cell counting of each mutant was performed in  
143 triplicates.

#### 144 **2.5 Cell dry weight analysis of the adhered cells after 48h**

145 After 48h, the silicone coupons with the developed biofilm on the surface have been taken out  
146 of the DFR and put into a 50 mL Falcon tube containing 10 mL of PBS. The biofilm was  
147 dissolved into the liquid through vigorous vortexing. Then, the dissolved biofilm has been  
148 gently sonicated (1 to 3 times for 40 sec with 30% of amplitude) to extract the surfactin  
149 molecules trapped in the biofilm matrix and dissolve the exopolysaccharides attached to the  
150 cells. After the sonication, the samples have been centrifuged. The supernatant was collected  
151 and the surfactin concentration was determined as described below (cf. 2.7). The cell pellets  
152 were washed by resuspending them in distilled water followed by centrifugation in order to  
153 eliminate the dissolved exopolysaccharides. The supernatant was discarded and the remaining  
154 cell pellet was re-dissolved in water and filtered (0.2  $\mu$ m). The filter with the retained cells has  
155 been dried in the oven at 105°C and weighted to determine the corresponding cell dry weight.

156 **2.6 Real-time observation of biofilm formation dynamics in the drip-flow reactor**

157 For a better understanding of the support colonization by the mutants, the biofilm development  
158 in the DFR has been visualized by a real-time camera. For this purpose, the plastic cover of the  
159 chamber was replaced by a purpose-made cover composed of an integrated fully transparent  
160 glass window for growth observation. Images were taken with a live camera every 15 min for  
161 the whole incubation time of 48h. The image sequence has been used to build a general  
162 colonization model.

163 **2.7 Surfactin production analysis**

164 Cell culture samples were taken after a total incubation time of 48h from the whole liquid phase  
165 that has passed and has been collected at each DFR chamber exit (~575 mL per chamber).  
166 Besides, the surfactin concentration has been determined in the sonicated biofilm samples (cf.  
167 section 2.5). The culture samples were centrifuged and the supernatant was filtered (0.2 µm)  
168 prior to the surfactin analysis by reversed-phase UPLC-MS (AQUITY UPLC H-Class, Waters,  
169 Zellik, Belgium) with an AQUITY UPLC BEH C-18 1.7 µm, 2.1x50mm, column (Waters,  
170 Zellik, Belgium) coupled to a single quadrupole MS (AQUITY SQ Detector, Waters, Zellik,  
171 Belgium). For sample ionization, the source temperature was set at 130°C with a desolvation  
172 temperature of 400°C, a nitrogen flow of 1000 L/h and a cone voltage of 120V. The UPLC  
173 analysis method was based on an acetonitrile/water gradient containing 0.1% formic acid with a  
174 flow rate of 0.6 mL/min and an analysis time of 7 min per sample. The elution was started at  
175 30% of acetonitrile. After 2.43 min acetonitrile was brought up to 95% and then again reduced  
176 to 30% at 5.1 min until the end.

177 Purified surfactin samples (>98%) (Lipofabrik, Villeneuve d'Ascq, France) were used to  
178 determine the retention time of the surfactin molecules and a calibration curve. Surfactin  
179 isomers were further identified through the recorded mass spectra. Specific m/z peaks were  
180 observed at 994, 1008, 1022, 1036, 1050 [M+H]<sup>+</sup> and 1016, 1030, 1044, 1058, 1072 [M+Na]<sup>+</sup>

181 representing the surfactin isomers C-12 to C-16 respectively. The overall surfactin  
182 concentration was calculated on the basis of the calibration curve.

## 183 **2.8 Statistical analysis**

184 Comparison of the cell dry weight and colony forming unit results between groups of *B. subtilis*  
185 mutants were performed using a pairwise two-tailed Student's t test. The differences between  
186 groups were considered as significant when  $p < 0.05$ .

## 187 **3 Results and discussion**

### 188 **3.1 Single cell phenotypic characterization of filamentous *B. subtilis* strains**

189 In the first part of this work, we looked at the dynamics of cell growth and spatial organization  
190 of the genetically engineered *B. subtilis* strains on agarose pads by time-lapse microscopy.  
191 Three main genetic targets have been selected, i.e. the introduction of a functional *sfp* gene  
192 necessary for lipopeptide synthesis, the restoration of the *epsC* gene required for the  
193 extracellular biofilm matrix production, and the deletion of the *sepF* gene involved in cell  
194 septation. This last mutation is known to impair cell septation leading to cell filamentation  
195 (Gündoğdu et al., 2011; Hamoen et al., 2006). The growth of isolated *B. subtilis* cells on  
196 agarose pads and the resulting microcolonies (single layer) have been tracked with a time-lapse  
197 microscope until the stationary growth phase was reached. As expected and already described  
198 by Hamoen et al. (2006), the deletion of *sepF* led to filamentous growth due to less efficient cell  
199 division. However, this deletion also had a considerable impact on the colony formation and  
200 colonization behavior. Cells with functional *sepF* (i.e. *B. subtilis* 168, BBG111 and RL5260)  
201 exhibited normal cell division dynamics which led to more packed colonies containing small  
202 cells that were easily distinguishable from each other with mean cell lengths comprised between  
203 3 to 6  $\mu\text{m}$ . For the filamentous strains containing the *sepF* deletion (i.e. *B. subtilis* TB92,  
204 BBG270 and BBG512), a less efficient cell division could be clearly observed in the  
205 exponential growth phase (~4h), leading to elongated cells that developed in length. After the

206 exponential growth phase, the filamentous cells also tended to separate. In the stationary phase  
207 at ~8h, maximum cell lengths of up to 26  $\mu\text{m}$  were observed with mean cell lengths comprised  
208 between 8 and 12  $\mu\text{m}$ . The strains with *sepF* deletion (TB92, BBG270 and BBG512) developed  
209 rather loosely packed micro-colonies with large spaces that were devoid of cells due to the  
210 filamentous cell growth. Consequently, they explored a larger area on the agarose surface by  
211 comparison with the *sepF+* strains. The increased colonization capacity was also observed for  
212 the filamentous surfactin producing strains BBG270 and BBG512 during macroscopic colony  
213 development on 0.7% agar LB plates. Hence, filamentous growth might be advantageous for a  
214 broader colonization of the bioreactor support material.

### 215 **3.2 Evaluation of colonization and biofilm formation capacity in a continuous drip-flow** 216 **reactor**

217 As a second characterization step, the engineered *B. subtilis* strains have been cultivated in a  
218 drip-flow reactor (DFR) in order to investigate the biofilm formation capacity on a solid inert  
219 support and under continuous nutrient supply.

#### 220 **3.2.1 Initial cell adhesion capacity**

221 Firstly, it was checked to what extent filamentous growth and EPS production is beneficial for  
222 the initial cell adhesion of surfactin producing *B. subtilis* strains on the DFR support. For this  
223 purpose, the bacterial cells present on the DFR support after 6h of batch phase followed by 1h  
224 of continuous flow have been counted. Therefore, the adhered cells have been detached and  
225 quantified by plate counting (Figure 2).

226 The initial cell adhesion capacities of the surfactin producing EPS+ strains (i.e. RL5260 (*sfp+*,  
227 *epsC+*) and BBG512 (*sfp+*, *epsC+*,  $\Delta\text{sepF}$ )) were up to ten-fold increased by comparison with  
228 the surfactin producing EPS deficient strains (i.e. BBG111 (*sfp+*) and BBG270 (*sfp+*,  $\Delta\text{sepF}$ )).  
229 EPS are natural polymers composed of sticky sugar substances that help the cells to adhere to a  
230 surface and to each other in the case of biofilm formation (Flemming et al., 2016; Vlamakis et  
231 al., 2013). However, no significant differences have been observed inside the groups (i.e.,

232 neither EPS+ nor EPS- strains), suggesting that cell filamentation upon deletion of *sepF* has no  
233 significant impact on the cell's initial adhesion in the surfactin producing strains.  
234 Regarding the non surfactin producing strains BS168 and TB92 ( $\Delta sepF$ ), the initial cell  
235 adhesion of the non-filamentous strain BS168 was slightly increased compared to the  
236 filamentous strain TB92. This negative impact of cell filamentation is probably linked to the  
237 less efficient cell division of TB92 which lead to coherent, not properly separated cells.  
238 Consequently, it is difficult to spread and plate single cells on the agar plate for a correct  
239 counting of the single colony forming units.

### 240 **3.2.2 Biofilm formation capacity**

241 In the next step, the engineered *B. subtilis* strains were incubated for 48h, including a 6h batch  
242 phase and 42h phase with continuous nutrient supply, until the development of a biofilm on the  
243 DFR coupon was observed. A schematic view of the used device is presented in **Figure 3A**.  
244 **Figure 3B** shows the coupons colonized by the different *B. subtilis* strains after 48h in the DFR.  
245 The corresponding amounts of cell dry weight that were measured in g per m<sup>2</sup> of coupon area  
246 are presented in **Figure 3C**. The surface structure of the silicone coupons used as support for the  
247 biofilm development in the DFR is presented in **Figure 3D**.

248 The induction of filamentous growth in the surfactin negative strain TB92 ( $\Delta sepF$ ) resulted in  
249 no significant increase in cell adhesion on the support compared to *B. subtilis* 168 (control), the  
250 cell adhesion capacities were similar. Since the silicone coupons possess a hydrophobic surface  
251 and these strains do not produce surfactin to decrease the surface tension, it is more difficult for  
252 the cells to spread. In this case, filamentous growth seemed to be neither advantageous nor  
253 unfavorable for the support colonization. Leclère et al. (2006) have already demonstrated that it  
254 is necessary to reduce the surface friction to increase the surface colonization capacity of  
255 *B. subtilis* 168. Surfactin is a surface-active agent that reduces the surface tension and thus  
256 permits the cells to spread more easily, as already shown by several authors (Coutte et al.,

257 2010a; Deleu et al., 1999; Julkowska et al., 2005, 2004; Kearns and Losick, 2003; Leclère et al.,  
258 2006).

259 The presence of surfactin showed a clear impact on the cell distribution on the coupon surfaces.  
260 The biofilm of the surfactin negative strains 168 and TB92 ( $\Delta sepF$ ) showed a clear front line on  
261 the coupon surface whereas the border regions of the surfactin producing strains BBG111  
262 ( $sfp+$ ) and BBG270 ( $sfp+$ ,  $\Delta sepF$ ) were smooth, an indicator for swarming motility due to the  
263 presence of surfactin (Kearns and Losick, 2003). The increased spreading capacity of BBG111  
264 and BBG270 due to the presence of surfactin led to the colonization of larger zones with a lesser  
265 cell density. Hence, the surfactin producing strains BBG111 ( $sfp+$ ) and BBG270 ( $sfp+$ ,  $\Delta sepF$ )  
266 were able to cover more homogenously the coupon surface by developing more smooth and  
267 better dispersed biofilms than the non surfactin producing strain BS168 or respectively TB92  
268 ( $\Delta sepF$ ).

269 However, the cell adhesion capacity of BBG111 ( $sfp+$ ) decreased two to three times compared  
270 to BS168. This occurred probably due to cell detachment and the washing out of cells through  
271 the presence of surfactin. But the cell adhesion capacity was recovered upon induction of  
272 filamentous growth (strain BBG270 ( $sfp+$ ,  $\Delta sepF$ )). The cell adhesion capacities of BBG270  
273 were up to three times higher than the ones of the strain BBG111 ( $sfp+$ ) and thus similar to the  
274 cell adhesion capacities of *B. subtilis* 168.

275 Regarding the initial cell adhesion after the batch phase (6h), the number of cells present on the  
276 coupons were similar for the filamentous strain BBG270 ( $sfp+$ ,  $\Delta sepF$ ) and non-filamentous  
277 strain BBG111 ( $sfp+$ ). Though, after 48h of incubation, the results have shown that provoked  
278 filamentous growth in the surfactin producing strain BBG270 permitted to increase up to three  
279 times the cell adhesion capacity resulting in a higher biomass adhered to the support material.

280 Möller et al. (2013) have already demonstrated that the colonization of heterogeneous surfaces  
281 under physiological flow conditions is accelerated in filamentous *E. coli* cells. The bacterial cell  
282 shape adaption resulted in an improved ability of bridging non-adhesive distances (Möller et al.,

283 2013). As the coupon surface analysis with the digital microscope has revealed, the silicone  
284 coupons consist of a rough surface with height differences of up to 42.5  $\mu\text{m}$  (cf. **Figure 3D**) that  
285 have an impact on the cell distribution and colonization. Probably, filamentous cells overcome  
286 more easily structural irregularities than small cells and consequently possess better  
287 colonization capacities. Furthermore, the formed cell aggregates of the filamentous cells seemed  
288 to have a better cohesion than the ones formed by small cells making the detaching and washing  
289 out of single cells more difficult, especially in the presence of surfactin. The advantages of the  
290 increased cohesion of filamentous cells is an interesting feature for biosurfactant production in  
291 biofilm reactors with *B. subtilis* strains to obtain a more efficient and stable colonization of the  
292 support materials and to reduce cell detachment from the biofilm.

293 The adhesion capacities of the strains with restored EPS production (RL5260 (*sfp+*, *epsC+*) and  
294 BBG512 (*sfp+*, *epsC+*,  $\Delta\text{sepF}$ )) increased 10 to 50 times compared to the strains displaying  
295 reduced EPS production (168, TB92, BBG111, BBG270). Moreover, the EPS+ mutants  
296 (RL5260 and BBG512) developed exceptional wrinkled biofilm structures on the DFR coupons.

297 The provoked cell filamentation in BBG512 (*sfp+*, *epsC+*,  $\Delta\text{sepF}$ ) showed no significant  
298 improvement in initial cell adhesion and biofilm formation after 48h of incubation compared to  
299 RL5260 (*sfp+*, *epsC+*).

300 As expected, the presence of EPS was a key factor for initial cell adhesion and biofilm  
301 formation on the drip-flow biofilm reactor support. These natural sticky compounds that are  
302 produced by the cells are involved in surface-cell and cell-to-cell interactions (Flemming et al.,  
303 2016; Marvasi et al., 2010; Vlamakis et al., 2013). Hence, the presence of EPS was found to  
304 increase the cell adhesion to a surprisingly high extent of up to 50-fold. No additional increase  
305 in cell adhesion was observed in EPS+ mutants with induced filamentous growth (BBG512),  
306 neither at the initial cell adhesion after 6h of incubation nor after 48h of incubation. However, it  
307 has to be considered that the cell adhesion was analyzed using a simple coupon surface. Biofilm  
308 bioreactors such as the previously mentioned trickle-bed biofilm reactor (Zune et al., 2013)

309 contain a highly structured packing with a very high specific surface area. In this case, probably,  
310 the cell adhesion capacities can be boosted much more through filamentous growth, even in  
311 EPS+ mutants. Obviously, the presence of EPS outcompeted the advantage of filamentous cells  
312 to colonize the silicone coupons due to an improved adhesion. Seminara et al. (2012)  
313 investigated the role of EPS in *B. subtilis* biofilm expansion. They found out that matrix  
314 production indeed contributes to biofilm spreading due to osmotic forces, probably to increase  
315 nutrient uptake. In this case, cell filamentation seemed to have a minor effect on biofilm  
316 formation than the EPS production.

317 In the EPS+ mutants (RL5260 and BBG512), the biofilm developed very complex wrinkled  
318 structures, characteristic of mature *B. subtilis* biofilms (Vlamakis et al., 2013). Moreover, a  
319 hydrophobic layer on the top of the biofilm was observed. The surface hydrophobicity of this  
320 protection layer is demonstrated by the colored water droplet staying at the top of the biofilm of  
321 RL5260 in **Figure 3B**. This hydrophobic layer is composed of the protein BslA, a hydrophobin  
322 that is synthesized in the last stages of biofilm maturation, as already described by several  
323 researchers (Arnaouteli et al., 2016; Kobayashi and Iwano, 2012; Mielich-Süss and Lopez,  
324 2015).

### 325 **3.2.3 Cell colonization and biofilm development mode in the drip-flow reactor**

326 As reported in the previous section (cf. 3.2.2), the EPS+ *B. subtilis* mutants (RL5260, BBG512)  
327 were able to develop remarkable wrinkled biofilm structures within 48h. Moreover, they were  
328 able to colonize the whole DFR coupon surface whereas the EPS deficient strains colonized  
329 only a part of the DFR coupons after 48h. Since the cell colonization and structural biofilm  
330 development on the DFR support seemed to be rather a heterogeneous phenomenon, the  
331 dynamics of biofilm formation has been studied. For this purpose, the biofilm formation has  
332 been tracked in real time with a camera placed in front of a window integrated in the chamber  
333 cover (cf. **Figure 3A**). A schematic representation of the biofilm development is presented in  
334 **Figure 4**. Several biofilm development stages on the DFR coupon (I-VI) have been identified



335 for the EPS+ mutants. Biofilm formation displayed by mutants with no EPS production stopped  
336 during the second development phase since there is neither a structural complex biofilm  
337 development nor a maturation phase. Mutants with restored EPS production reached the last  
338 phase showing a structurally complex and mature biofilm covering the whole coupon. The  
339 biofilm formation took place according to the generally recognized biofilm developing steps:  
340 attachment – growth of micro- and macro-colonies – biofilm maturation – cell detachment and  
341 dispersion (Vlamakis et al., 2013). However, in the beginning, the surface conditioning and  
342 nutrient delivery was crucial for cell development. The cells only started to develop where the  
343 bulk medium was passing on the coupon. Since the medium had a quite low flow rate of  
344 ~13 mL/h, it entered only dropwise into the cultivation chamber and then flowed down  
345 randomly on the coupon surface. This means that not the complete coupon surface was  
346 continuously delivered by fresh medium. Consequently, the coupon became only partly  
347 colonized by a biofilm. The development of this first biofilm until its complete maturation  
348 required 18-20h of incubation in the continuous mode preceding 6h of batch phase. Due to the  
349 maturation, a hydrophobic protein layer covered the biofilm. This special feature of *B. subtilis*  
350 biofilms has already been mentioned previously in the upper part and demonstrated through the  
351 colored water droplet staying on the biofilm surface in **Figure 3B**. Since the hydrophobic  
352 surface became impervious to the bulk medium, the latter one bypassed to uncolonized surfaces  
353 on the coupon. This gave the starting point for a new biofilm development of dispersed cells  
354 until the whole coupon was colonized by multiple biofilms. Actually, the mature biofilm at the  
355 end of the cultivation (~ 40h) was composed of several associated biofilms with different ages  
356 and maturations stages.

357 In EPS+ mutants, a mature biofilm with complex wrinkled structures could be observed after  
358 20h of continuous nutrient supply in the DFR, a complete colonization of the DFR coupon was  
359 achieved after around 40h, whereas EPS deficient mutants were neither able to develop an  
360 architecturally complex biofilm structure nor to colonize completely the DFR coupon. Besides,  
361 it has been demonstrated that EPS gave structural integrity to the biofilm and triggered its

362 maturation through the formation of a hydrophobic protection layer. Although the biofilm  
363 matrix provides advantages in biofilm-based processes like increased adhesion capacities and  
364 protection from external forces such as shear forces or pH changes, there are also some  
365 drawbacks. The hydrophobic protection layer which is formed by *B. subtilis* at the final  
366 maturation stage through the secretion of the hydrophobin BslA represents an effective barrier  
367 that prevents the penetration of gas and liquids (Arnaouteli et al., 2016). This may provoke  
368 undesirable nutrient limitations during fermentations in biofilm bioreactors with *B. subtilis*.

### 369 **3.3 Enhanced biofilm formation leads to higher surfactin production**

370 After characterizing the cell adhesion and colonization of the support, the resulting surfactin  
371 production has been analyzed using UPLC-MS as described in section 2.7. Hence, after 48h of  
372 incubation, the surfactin concentration was measured in the biofilm as well as in the supernatant  
373 of the liquid passing the reactor chamber with a total volume of ~575 mL. The measured  
374 amounts of surfactin are presented in Table 2. Surfactin was mainly present in the liquid phase  
375 and only in small amounts in the biofilm.

376 Apparently, the surfactin molecules released by the cells were effectively flushed out by the  
377 passing medium, only a low amount stayed trapped in the biofilm.

378 BBG111 (*sfp+*) and BBG270 (*sfp+*,  $\Delta sepF$ ) produced comparable amounts of surfactin, as well  
379 as RL5260 (*sfp+*, *epsC+*) and BBG512 (*sfp+*, *epsC+*,  $\Delta sepF$ ), suggesting that the deletion of  
380 *sepF* has no detrimental impact on surfactin production. Globally, the surfactin production in  
381 the EPS+ strains was 8 to 10 times higher than in the EPS deficient strains as the number of  
382 adhered cells was also increased (10 to 50 times) compared to the EPS deficient strains.

## 383 **4 Conclusions**

384 In this work, genetic engineering strategies to improve support colonization in biofilm  
385 cultivations with *B. subtilis* 168 are presented. The support colonization capacity was three  
386 times increased in surfactin producing mutants through the induction of cell filamentation. The

387 presence of EPS improved up to 50 times the support colonization whereby cell filamentation  
388 had a minor impact. EPS were essential for the initial cell adhesion and for giving structural  
389 integrity to the cells in the biofilm. The *B. subtilis* mutants are potential candidates for the future  
390 use in biofilm bioreactors to achieve an enhanced support colonization for an increased  
391 lipopeptide productivity.

392

393 E-supplementary data for this work can be found in e-version of this paper online.

394

### 395 **Acknowledgement**

396 This research received funding from the European INTERREG Va SmartBioControl / BioProd  
397 project and the ALIBIOTECH program funding administered by the Hauts-de-France Region.

398 Met steun van het europees fonds voor regionale ontwikkeling. Avec le soutien du fonds  
399 européen de développement régional.

400 HB is supported by an international PhD grant co-funded by the Université de Liège and the  
401 Hauts-de-France Region. The authors are grateful to Prof. Leendert Hamoen from the  
402 University of Amsterdam for donation of the *B. subtilis* TB92 strain and Prof. Richard Losick  
403 from Harvard University for donation of the *B. subtilis* RL5260 strain. Furthermore, we would  
404 like to thank Jean-François Willaert (Gembloux Agro-Bio Tech – Université de Liège) for his  
405 technical assistance for the purpose-made DFR covers used for the biofilm growth observation  
406 as well as Andrew Zicler (Gembloux Agro-Bio Tech – Université de Liège) for his help with  
407 some of the figures.

408

### 409 **Conflict of interest**

410 The authors have declared no conflict of interest.

## 5 References

1. Arnaouteli, S., Macphee, C.E., Stanley-wall, N.R., 2016. Just in case it rains: building a hydrophobic biofilm the *Bacillus subtilis* way. *Curr. Opin. Microbiol.* 34, 7–12.  
<https://doi.org/10.1016/j.mib.2016.07.012>
2. Branda, S.S., Gonza, E., Dervyn, E., Ehrlich, S.D., Losick, R., Kolter, R., 2004. Genes Involved in Formation of Structured Multicellular Communities by *Bacillus subtilis*. *J. Bacteriol.* 186, 3970–3979. <https://doi.org/10.1128/JB.186.12.3970>
3. Chtioui, O., Dimitrov, K., Gancel, F., Dhulster, P., Nikov, I., 2012. Rotating discs bioreactor, a new tool for lipopeptides production. *Process Biochem.* 47, 2020–2024.  
<https://doi.org/10.1016/j.procbio.2012.07.013>
4. Coutte, F., Leclère, V., Béchet, M., Guez, J.S., Lecouturier, D., Chollet-Imbert, M., Dhulster, P., Jacques, P., 2010a. Effect of *pps* disruption and constitutive expression of *surfA* on surfactin productivity, spreading and antagonistic properties of *Bacillus subtilis* 168 derivatives. *J. Appl. Microbiol.* 109, 480–491. <https://doi.org/10.1111/j.1365-2672.2010.04683.x>
5. Coutte, F., Lecouturier, D., Dimitrov, K., Guez, J., Delvigne, F., Dhulster, P., Jacques, P., 2017. Microbial lipopeptide production and purification bioprocesses, current progress and future challenges. *Biotechnol. J.* 12, 1–10.  
<https://doi.org/10.1002/biot.201600566>
6. Coutte, F., Lecouturier, D., Leclère, V., Béchet, M., Jacques, P., Dhulster, P., 2013. New integrated bioprocess for the continuous production, extraction and purification of lipopeptides produced by *Bacillus subtilis* in membrane bioreactor. *Process Biochem.* 48, 25–32. <https://doi.org/10.1016/j.procbio.2012.10.005>
7. Coutte, F., Lecouturier, D., Yahia, S.A., Leclère, V., Béchet, M., Jacques, P., Dhulster, P., 2010b. Production of surfactin and fengycin by *Bacillus subtilis* in a bubbleless membrane bioreactor. *Appl. Microbiol. Biotechnol.* 87, 499–507.

- <https://doi.org/10.1007/s00253-010-2504-8>
8. Deleu, M., Razafindralambo, H., Popineau, Y., Jacques, P., Thonart, P., Paquot, M., 1999. Interfacial and emulsifying properties of lipopeptides from *Bacillus subtilis*. *Colloids Surf. A Physicochem. Eng. Asp.* 152, 3–10.
  9. Ercan, D., Demirci, A., 2015. Current and future trends for biofilm reactors for fermentation processes. *Crit. Rev. Biotechnol.* 35, 1–14.  
<https://doi.org/10.3109/07388551.2013.793170>
  10. Fahim, S., Dimitrov, K., Vauchel, P., Gancel, F., Delaplace, G., Jacques, P., Nikov, I., 2013. Oxygen transfer in three phase inverse fluidized bed bioreactor during biosurfactant production by *Bacillus subtilis*. *Biochem. Eng. J.* 76, 70–76.  
<https://doi.org/10.1016/j.bej.2013.04.004>
  11. Flemming, H.-C., Wingender, J., Szewzyk, U., Steinberg, P., Rice, S.A., Kjelleberg, S., 2016. Biofilms : an emergent form of bacterial life. *Nat. Rev. Microbiol.* 14, 563–575.  
<https://doi.org/10.1038/nrmicro.2016.94>
  12. Gündoğdu, M.E., Kawai, Y., Pavlendova, N., Ogasawara, N., Errington, J., Scheffers, D.-J., Hamoen, L.W., 2011. Large ring polymers align FtsZ polymers for normal septum formation. *EMBO J.* 30, 617–626. <https://doi.org/10.1038/emboj.2010.345>
  13. Hamoen, L.W., Meile, J.C., De Jong, W., Noirot, P., Errington, J., 2006. SepF, a novel FtsZ-interacting protein required for a late step in cell division. *Mol. Microbiol.* 59, 989–999. <https://doi.org/10.1111/j.1365-2958.2005.04987.x>
  14. Jacques, P., 2011. Surfactin and Other Lipopeptides from *Bacillus spp.*, in: Soberón-Chávez, G. (Ed.), *Biosurfactants, Microbiology Monographs*. Springer Verlag Berlin Heidelberg, Berlin Heidelberg, pp. 57–91.  
<https://doi.org/10.1017/CBO9781107415324.004>
  15. Jong, I.G. De, Beilharz, K., Kuipers, O.P., Veening, J.-W., 2011. Live Cell Imaging of *Bacillus subtilis* and *Streptococcus pneumoniae* using Automated Time-lapse Microscopy. *J. Vis. Exp.* 53, 1–6. <https://doi.org/10.3791/3145>

16. Julkowska, D., Obuchowski, M., Holland, I.B., Se, S.J., 2005. Comparative Analysis of the Development of Swarming Communities of *Bacillus subtilis* 168 and a Natural Wild Type : Critical Effects of Surfactin and the Composition of the Medium. *J. Bacteriol.* 187, 65–76. <https://doi.org/10.1128/JB.187.1.65>
17. Julkowska, D., Obuchowski, M., Holland, I.B., Séror, S.J., 2004. Branched swarming patterns on a synthetic medium formed by wild-type *Bacillus subtilis* strain 3610 : detection of different cellular morphologies and constellations of cells as the complex architecture develops. *Microbiology* 1839–1849. <https://doi.org/10.1099/mic.0.27061-0>
18. Kearns, D.B., Chu, F., Branda, S.S., Kolter, R., Losick, R., 2005. A master regulator for biofilm formation by *Bacillus subtilis*. *Mol. Microbiol.* 55, 739–749. <https://doi.org/10.1111/j.1365-2958.2004.04440.x>
19. Kearns, D.B., Losick, R., 2003. Swarming motility in undomesticated *Bacillus subtilis*. *Mol. Microbiol.* 49, 581–590. <https://doi.org/10.1046/j.1365-2958.2003.03584.x>
20. Khalesi, M., Zune, Q., Telek, S., Riveros-Galan, D., Verachtert, H., Toye, D., Gebruers, K., Derdelinckx, G., Delvigne, F., 2014. Fungal biofilm reactor improves the productivity of hydrophobin HFBII. *Biochem. Eng. J.* 88, 171–178. <https://doi.org/10.1016/j.bej.2014.05.001>
21. Kobayashi, K., Iwano, M., 2012. BslA(YuaB) forms a hydrophobic layer on the surface of *Bacillus subtilis* biofilms. *Mol. Microbiol.* 85, 51–66. <https://doi.org/10.1111/j.1365-2958.2012.08094.x>
22. Leclère, V., Marti, R., Béchet, M., Fickers, P., Jacques, P., 2006. The lipopeptides mycosubtilin and surfactin enhance spreading of *Bacillus subtilis* strains by their surface-active properties. *Arch. Microbiol.* 186, 475–483. <https://doi.org/10.1007/s00203-006-0163-z>
23. Marvasi, M., Visscher, P.T., Casillas Martinez, L., 2010. Exopolymeric substances (EPS) from *Bacillus subtilis*: polymers and genes encoding their synthesis. *FEMS Microbiol. Lett.* 313, 1–9. <https://doi.org/10.1111/j.1574-6968.2010.02085.x>

24. McLoon, A.L., Guttenplan, S.B., Kearns, D.B., Kolter, R., Losick, R., 2011. Tracing the domestication of a biofilm-forming bacterium. *J. Bacteriol.* 193, 2027–2034.  
<https://doi.org/10.1128/JB.01542-10>
25. Mielich-Süss, B., Lopez, D., 2015. Molecular mechanisms involved in *Bacillus subtilis* biofilm formation. *Environ. Microbiol.* 17, 555–565. <https://doi.org/10.1111/1462-2920.12527>
26. Möller, J., Emge, P., Vizcarra, I.A., Kollmannsberger, P., Vogel, V., 2013. Bacterial filamentation accelerates colonization of adhesive spots embedded in biopassive surfaces. *New J. Phys.* 15, 1–19. <https://doi.org/10.1088/1367-2630/15/12/125016>
27. Seminara, A., Angelini, T.E., Wilking, J.N., Vlamakis, H., Ebrahim, S., Kolter, R., Weitz, D.A., Brenner, M.P., 2012. Osmotic spreading of *Bacillus subtilis* biofilms driven by an extracellular matrix. *Proc. Natl. Acad. Sci.* 109, 1116–1121.  
<https://doi.org/10.1073/pnas.1109261108>
28. Tanaka, K., Henry, C.S., Zinner, J.F., Jolivet, E., Cohoon, M.P., Xia, F., Bidnenko, V., Ehrlich, S.D., Stevens, R.L., Noirot, P., Micalis, U.M.R., Micalis, U.M.R., 2012. Building the repertoire of dispensable chromosome regions in *Bacillus subtilis* entails major refinement of cognate large-scale metabolic model. *Nucleic Acids Res.* 1–13.  
<https://doi.org/10.1093/nar/gks963>
29. Vlamakis, H., Chai, Y., Beauregard, P., Losick, R., Kolter, R., 2013. Sticking together: building a biofilm the *Bacillus subtilis* way. *Nat. Rev. Microbiol.* 11, 157–168.  
<https://doi.org/10.1038/nrmicro2960>
30. Volke, D.C., Nickel, P.I., 2018. Getting Bacteria in Shape: Synthetic Morphology Approaches for the Design of Efficient Microbial Cell Factories. *Adv. Biosyst.* 1800111, 1–21. <https://doi.org/10.1002/adbi.201800111>
31. Zhao, L., Ye, J., Fu, J., Chen, G.Q., 2018. Engineering peptidoglycan degradation related genes of *Bacillus subtilis* for better fermentation processes. *Bioresour. Technol.* 248, 238–247. <https://doi.org/10.1016/j.biortech.2017.05.134>

32. Zune, Q., Delepierre, A., Gofflot, S., Bauwens, J., Twizere, J.C., Punt, P.J., Francis, F., Toye, D., Bawin, T., Delvigne, F., 2015. A fungal biofilm reactor based on metal structured packing improves the quality of a *Gla::GFP* fusion protein produced by *Aspergillus oryzae*. *Appl. Microbiol. Biotechnol.* 99, 6241–6254.  
<https://doi.org/10.1007/s00253-015-6608-z>
33. Zune, Q., Soyeurt, D., Toye, D., Ongena, M., Thonart, P., Delvigne, F., 2013. High-energy X-ray tomography analysis of a metal packing biofilm reactor for the production of lipopeptides by *Bacillus subtilis*. *J. Chem. Technol. Biotechnol.* 89, 382–390.  
<https://doi.org/10.1002/jctb.4128>
34. Zune, Q., Telek, S., Calvo, S., Salmon, T., Alchihab, M., Toye, D., Delvigne, F., 2017. Influence of liquid phase hydrodynamics on biofilm formation on structured packing : Optimization of surfactin production from *Bacillus amyloliquefaciens*. *Chem. Eng. Sci.* 170, 628–638. <https://doi.org/10.1016/j.ces.2016.08.023>



## Figure captions

**Figure 1:** Molecular strategies to obtain a lipopeptide producing *B. subtilis* 168 strain adapted to biofilm cultivation mode: (I) insertion of a functional *sfp* gene (Coutte et al., 2010a), (II) restoration of the *epsC* gene (McLoon et al., 2011), (III) provoking of filamentous growth through the gene deletion of *sepF* (Hamoen et al., 2006).

**Figure 2:** Initial cell adhesion capacity of the *B. subtilis* strains on the DFR coupons. Samples were taken after an incubation time of 6h (batch phase) followed by 1h of continuous flow (~13 mL/h) to flush gently away non-adhering cells in the DFR. The counted numbers of colony forming units are presented with the corresponding standard deviation. Significant differences ( $p < 0.05$ ) between groups are indicated by small letters (a, b or c).

**Figure 3:** (A) Schematic view of the drip-flow cultivation device with six parallel growth chambers. Each chamber contains a coupon for evaluating biofilm development; An integrated glass window allows real-time analysis of the biofilm development. (B) Cell adhesion and biofilm formation capacities of the engineered *B. subtilis* strains on a silicone coupon in the DFR. A colored water droplet was placed on the top of the biofilm formed by RL5260 as an indicator for hydrophobicity. (C) Measured amount of cell dry weight in g per m<sup>2</sup> of coupon area. The values are represented with the corresponding standard deviation. Significant differences ( $p < 0.05$ ) between groups are indicated by small letters (a, b or c). (D) Structure of the uncolonized silicone coupon surface recorded with a 3D high resolution digital microscope.

**Figure 4:** Scheme displaying cell colonization and biofilm development over time on the silicone coupons in the DFR. The arrows in dark blue indicate which biofilm development stage was reached by the different engineered *B. subtilis* strains.

## Tables

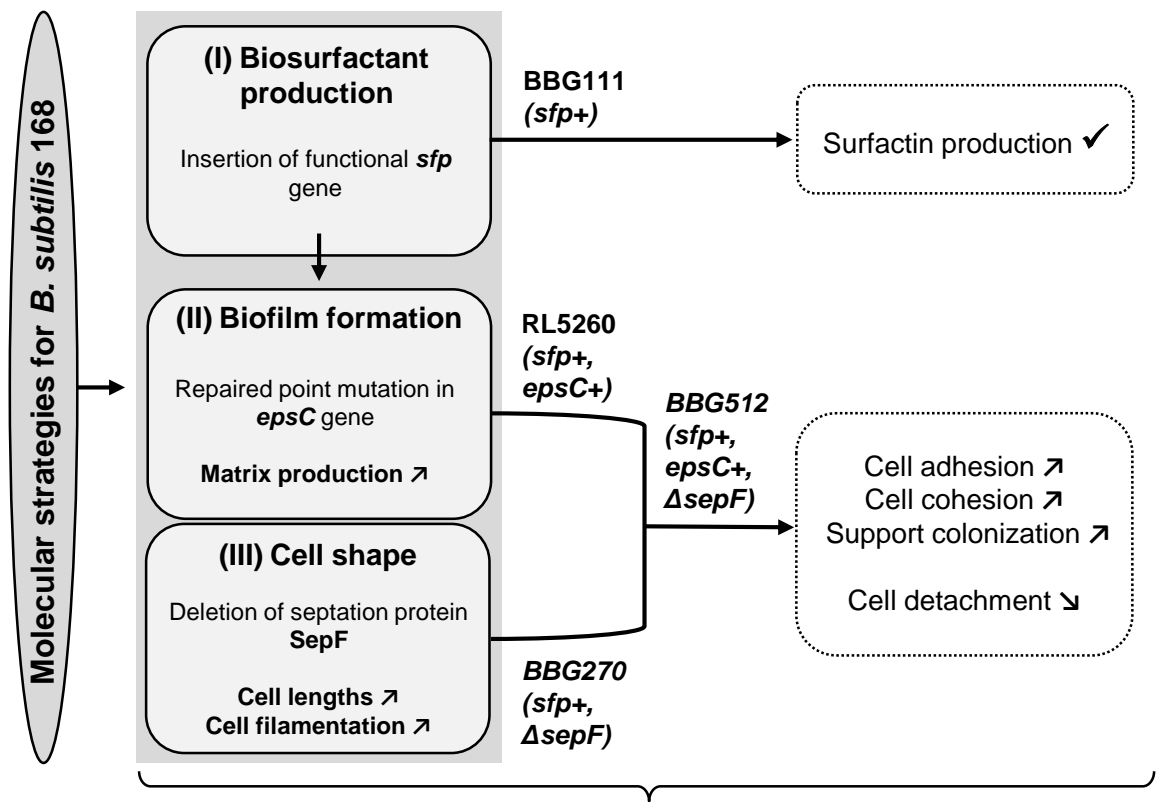
**Table 1: Bacterial strains and plasmids used in this study.**

Strains or plasmids	Genotype or plasmid composition	Source
<i>Bacterial strains</i>		
<b><i>Escherichia coli</i> JM109</b>	<i>endA1, recA1, gyrA96, thi, hsdR17</i> ( $\Gamma_k$ , $m_k^+$ ), <i>relA1, supE44, <math>\Delta(lac-proAB)</math>, [F'<i>traD36, proAB, laqI</i><sup>qZ</sup><math>\Delta</math>M15]</i>	Promega Corporation
<b><i>Bacillus subtilis</i> 168</b>	<i>trpC2</i>	Lab stock
<b>TB92</b>	<i>trpC2, <math>\Delta sepF::Spc^R</math> (derived from 168)</i>	(Hamoen et al., 2006)
<b>BBG111</b>	<i>trpC2, amyE::sfp-Cm<sup>R</sup> (derived from 168)</i>	(Coutte et al., 2010a)
<b>BBG270</b>	<i>trpC2, <math>\Delta sepF::Spc^R</math>, amyE::sfp-Cm<sup>R</sup> (derived from TB92)</i>	This study
<b>RL5260</b>	<i>trpC2, epsC+, sfp+, Erm<sup>R</sup></i>	(McLoon et al., 2011)
<b>Master strain BBG501</b>	<i>trpC2, epsC+, sfp+, Erm<sup>R</sup>, <math>\Delta upp::P\lambda</math>-Neo<sup>R</sup> (derived from RL5260)</i>	This study
<b>BBG512</b>	<i>trpC2, epsC+, sfp+, Erm<sup>R</sup>, <math>\Delta upp::P\lambda</math>-Neo<sup>R</sup>, <math>\Delta sepF::Phleo^R</math>-upp-cl (derived from BBG501)</i>	This study
<i>Plasmids</i>		
<b>pGEM®-T Easy</b>	Cloning vector	Promega Corporation
<b>pBG129</b>	<i>amyE-sfp-Cm<sup>R</sup>-amyE-Spc<sup>R</sup> cloned into pGEM®-T Easy</i>	(Coutte et al., 2010a)
<b>pBG402</b>	<i>upp<sup>UP</sup>-<math>\lambda</math>Pr-Neo<sup>R</sup>-upp<sup>DOWN</sup> cloned into pGEM®-T Easy</i>	This study

**Table 2: Surfactin production and productivity of the engineered strains grown in continuous DFR biofilm cultures after 48h of cultivation with the corresponding standard deviation.**

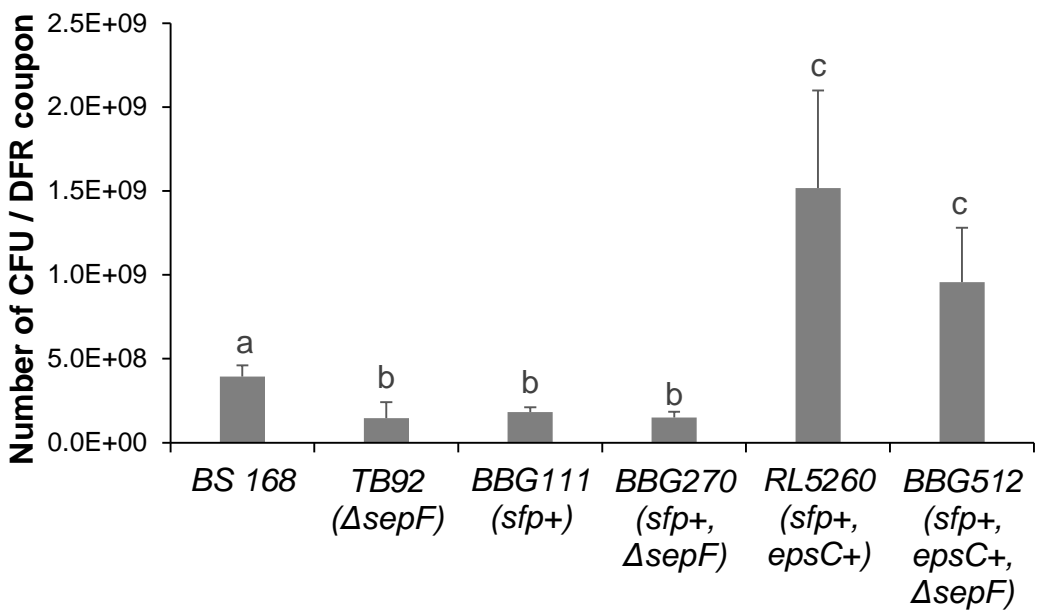
	<i>BBG111</i> ( <i>sfp+</i> )	<i>BBG270</i> ( <i>sfp+</i> , $\Delta$ <i>sepF</i> )	<i>RL5260</i> ( <i>sfp+</i> , <i>epsC+</i> )	<i>BBG512</i> ( <i>sfp+</i> , <i>epsC+</i> , $\Delta$ <i>sepF</i> )
<b>Surfactin production in the liquid phase after 48h [mg/L]</b>	7.42 ± 2.26	7.20 ± 2.56	70.64 ± 28.05	56.23 ± 22.80
<b>Amount of surfactin present in the biofilm after 48h [mg]</b>	0.02 ± 0.02	0.06 ± 0.04	0.66 ± 0.20	0.60 ± 0.38
<b>Surfactin productivity per DFR chamber [mg/h]</b>	0.09 ± 0.03	0.09 ± 0.03	0.85 ± 0.34	0.67 ± 0.27

Figure 1



Continuous surfactin production through naturally immobilized cells of *B. subtilis* 168

**Figure 2**



**Figure 3**

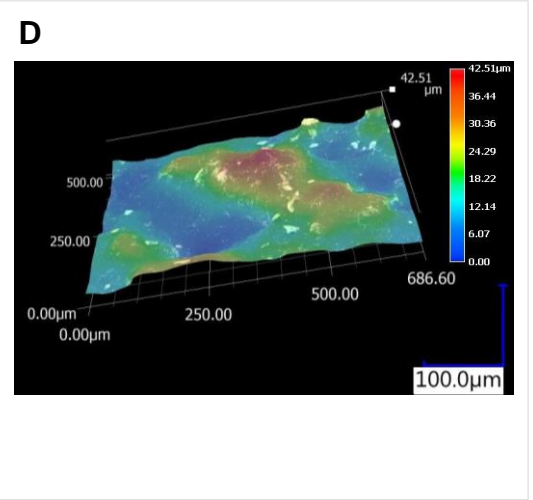
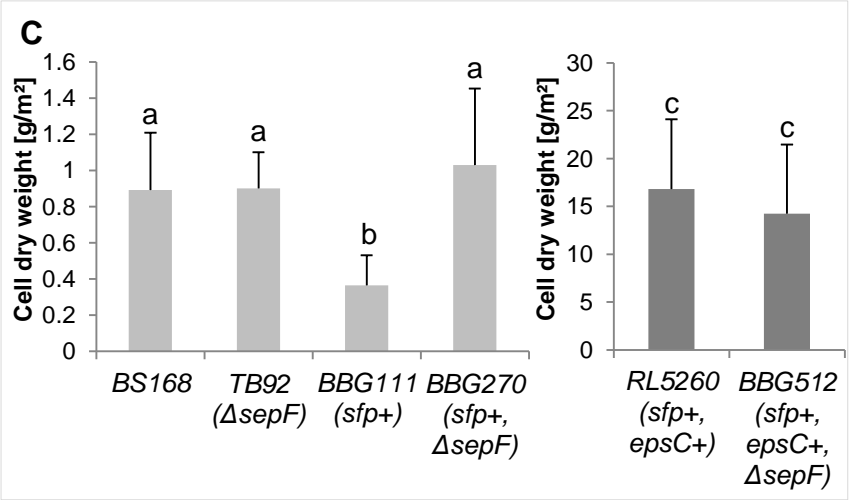
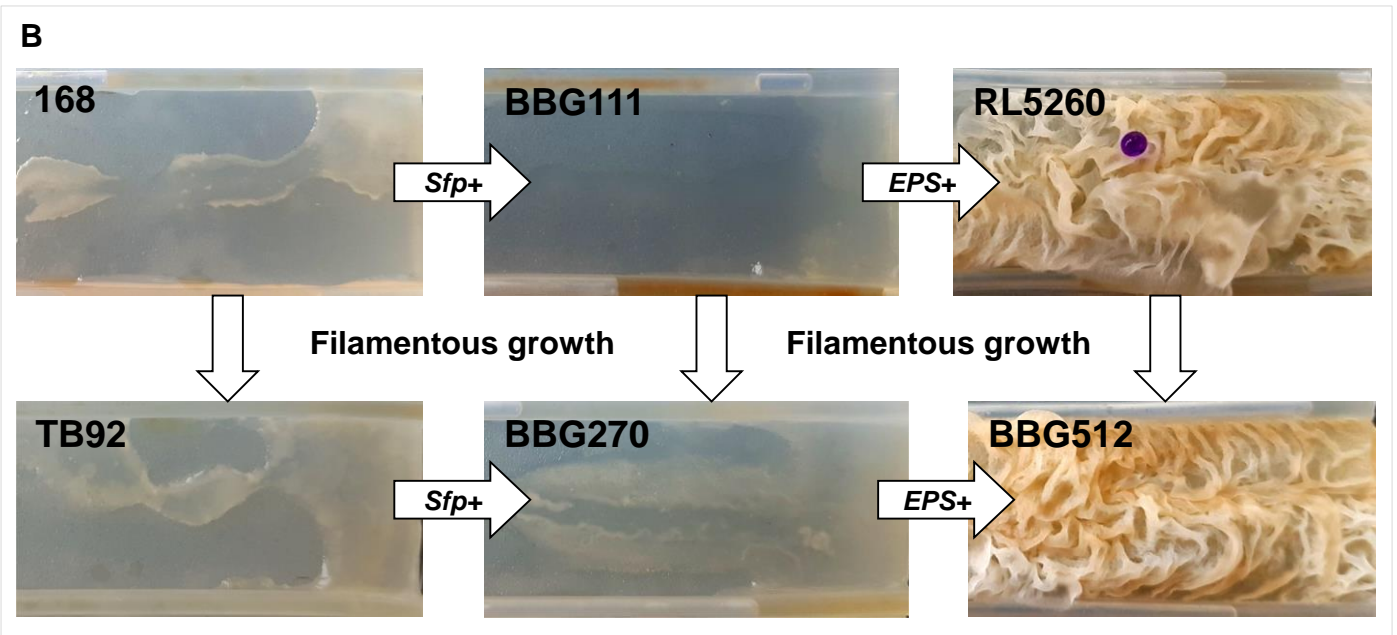
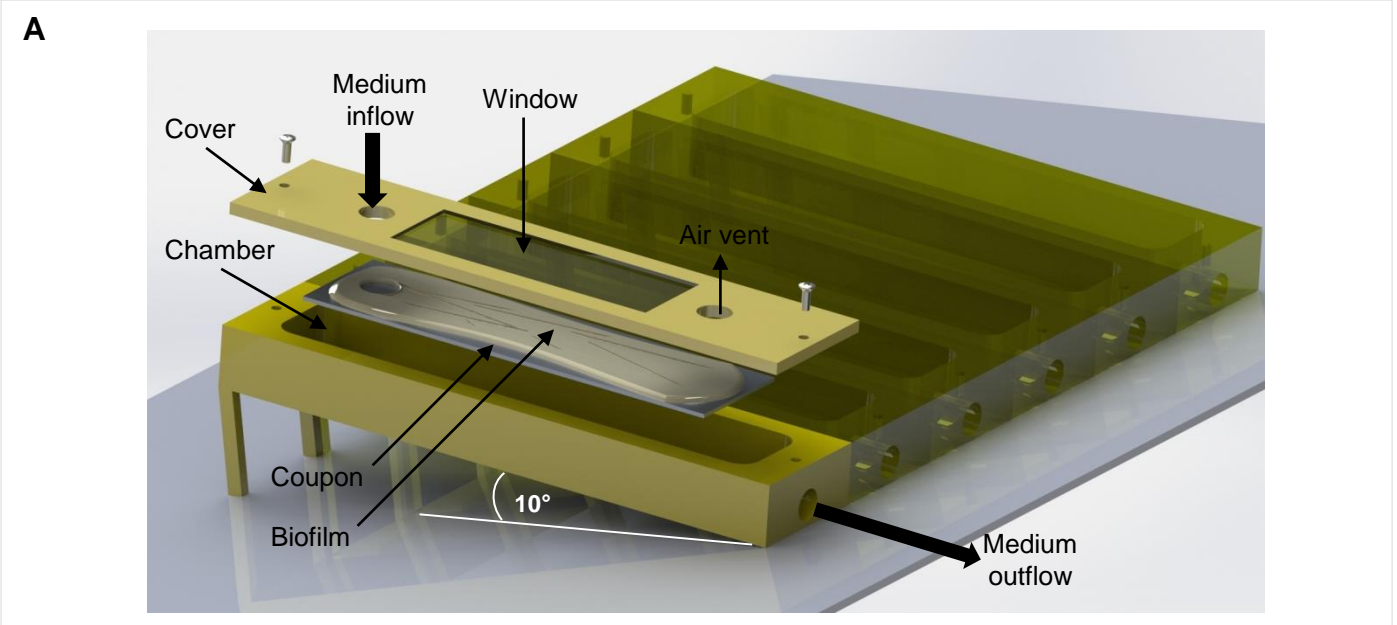


**Figure 4**

